Adaptive Model Predictive Control of an Interleaved Boost Converter Using Real-Time Updated Model

Hongyu Zhang, *Student Member, IEEE*, Yuren Li, Renyou Xie, *Student Member, IEEE*, Jian Song, *Student Member, IEEE*, Bo Liang, and Yigeng Huangfu, *Senior Member, IEEE*

***Abstract*—To optimize the voltage regulation performance and enhance the robustness, an adaptive model predictive controller is proposed in this article for an interleaved dc–dc boost converter. The predictive model is constructed by linearizing the nonlinear equations of the converter at the current operating point. A novel parameter update mechanism is developed based on the static model, which enables fast and accurate identification of the model parameters, thus the control law can guarantee the desired control performance in the wide operating range. Based on the adaptive model, a disturbance observer is constructed to correct the model predictions and mitigate parameter uncertainties. Then an explicit control law is derived by solving the optimization problem offline, and the stability analysis is carried out using the linear control theory. Finally, the effectiveness of the proposed method is verified by both simulation and experimental results.**

***Index Terms*—Disturbance observer (DOB), interleaved boost converter, model predictive control (MPC), offset-free tracking.**

I. Introduction

RAPID development in renewable energy has promoted the utilization of power converters. Since the output voltage of renewable energy sources, such as fuel cells and photovoltaics is low and unregulated, power converters are required as the interfaces for energy sources and loads. Among them, the interleaved boost converter is a promising candidate due to its superiorities in power density, efficiency, and fault tolerance [1]. However, the nonminimum phase behaviors and random load variations of the converter bring great difficulties to its accurate control. Thus, many advanced control strategies have been developed such as backstepping control [2], sliding mode control [3], flatness control [4], etc. The existing methods have improved the control performance from different aspects.

Among different control methods, model predictive control (MPC) is known as one of the most promising approaches in industrial applications, due to its optimized control effects with a flexible and straightforward design process [5], [6]. Restricted by the computational burden, MPC was originally applied to the process control with slow time-varying dynamics [7]. With the development of computing hardware and optimization method, MPC has been successfully applied in power electronics, such as neutral-point-clamped inverters [8], [9], servo motors [10], and power converters/rectifiers [11], [12]. Moreover, literature [13] implements an MPC method with a long horizon on a field-programmable gate array (FPGA), which further promotes the application of MPC in fast dynamic systems.

As a model-based method, the performance of MPC greatly depends on the accuracy of the system model. The insufficient knowledge of model parameters and other unmodeled dynamics will cause prediction errors and guide the control system along a different trajectory from the reference one. For this reason, the integral action was integrated into MPC to mitigate steady-state errors [14]. Note that the integral action also interacts with other control performances, such as transient behaviors, tracking, and robustness. Thus, applying integral action to mitigate the offset may deteriorate the other properties of the closed-loop system. Numerous efforts have been made to remove the control offsets of MPC, which motivates the design of adaptive MPC (AMPC). In general, the realization of AMPC can be divided into model approximation, adaptation techniques, parameter identification, and disturbance estimation methods.

For model approximation methods, the system dynamics are approximated by a set of submodels. Therefore, the parameter uncertainties could be captured in the wide operating range. In [15], a parameter-varying model consisting of a set of linearized models at different operating points was applied to describe the converter dynamics. In [16], the authors developed an AMPC for modular multilevel converters, and a fuzzy approximation system with adaptive weight vectors was applied to estimate the unknown nonlinear system dynamics based on the input/output data. However, in [15] and [16], the prediction accuracy is affected by the number of submodels, and the model parameters cannot exceed the predefined minimum/maximum ranges. The AMPC with adaptation techniques normally utilizes adaptive updating laws to estimate the sensitive parameters of the system. In [17], an AMPC was proposed for discrete-time linear systems, and the adaptive law for model parameters was developed based on the gradient descent method. Some other adaptation laws were designed and integrated into AMPCs for servo motors, such

Manuscript received 28 May 2022; revised 6 September 2022; accepted 17 October 2022. Date of publication 25 October 2022; date of current version 18 November 2022. This work was supported in part by the Key Research and Development Program of Shaanxi under Grant 2021GY-292, in part by the Aviation Science Foundation under Grant ASFC-20200019053004, and in part by the National Natural Science Foundation of China under Grant 61873343. Recommended for publication by Associate Editor J. Popovic-Gerber. *(Corresponding author: Yuren Li.)*

The authors are with the School of Automation, Northwestern Polytechnical University, Xi'an 710129, China (e-mail: hongyu.zhang@mail.nwpu.edu.cn; liyuren@nwpu.edu.cn; xierenyou@mail.nwpu.edu.cn; jiansong@mail.nwpu.edu.cn; liangbo@nwpu.edu.cn; yigeng@nwpu.edu.cn).

Color versions of one or more figures in this article are available at https://doi.org/10.1109/TPEL.2022.3216600.

Digital Object Identifier 10.1109/TPEL.2022.3216600

as the Lyapunov method [18], and the Popov hyperstability theory [19]. But for this kind of AMPC, the algorithm complexity will increase with the number of sensitive model parameters. Some online parameter identification laws are also used to identify the model parameters in the prediction model. These algorithms do not require prior knowledge of the control plants. In [20], a predictive control was proposed for power converters, and the pseudo-partial derivative was updated by a data-driven iterative learning method. In [21], an AMPC with neuro-fuzzy parameter estimation was developed for the grid-forming converters. The recursive least squares (RLS) algorithm was used to identify the predictive model in [22]. The main disadvantage of [20], [21], [22] is the utilization of complex and computationally intensive algorithms and high data storage requirements. To address this problem, an adaptive reference MPC was developed in [23] to reduce the computation costs. It models the virtual system using the linear fitting method, and a virtual reference is generated to mitigate mismatches, which has better transient performance than MPC with integrator. Except for these AMPCs mentioned above, disturbance estimation is also an efficient method to deal with model mismatches, and some AMPCs are implemented by applying disturbance observers (DOB). In [24], the Luenberger observer was adopted to estimate the input voltage and inductor resistance. The Luenberger observer was also applied in [25] to estimate the load resistance, thus the developed AMPC method exhibited strong robustness against load variations.

The AMPC works mentioned above can enhance the control performance and robustness to certain mismatched parameters. However, for boost converters, the consideration of parameter mismatches is not comprehensive, such as the negative effects caused by the nonminimum phase behaviors and variations in inductance. Besides, it should be noted that the AMPC works described above mainly focus on dealing with the parameter uncertainties under normal operating conditions, and few works have been extended to suppress parameter uncertainties and guarantee the optimized control performance under circuit fault conditions.

To address the aforementioned problems, this article proposes a composite AMPC law that combines parameter identification and an observer for interleaved boost converters. The adaptive predictive model consists of two units, the linear model and the lumped disturbance term. A novel parameter update mechanism is proposed to identify the model parameters. Different from the existing identification laws, the parameter update mechanism is developed based on the static model, which enables fast and accurate parameter identification with low computational costs. Based on the adaptive model, a DOB is adopted to compensate for the lumped disturbances, including the non-minimum phase behaviors, linearization errors, and other parasitic parameters. Finally, an explicit closed-loop solution is obtained by solving the receding horizon optimization problem offline.

The main contributions of this article include the following:

1) A novel parameter update mechanism is developed based on the static model, which enables fast and accurate parameter identification with low computational costs in the presence of large external disturbances.

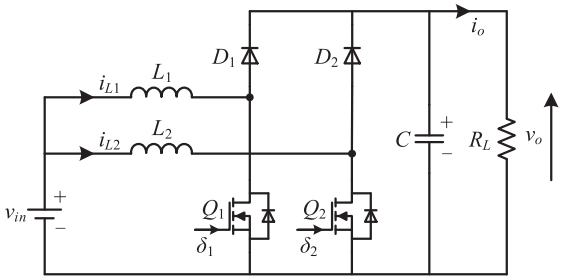

Fig. 1. Topology of TIBC.

2) The proposed method takes the circuit fault conditions into account, thus generating the optimized control performance over a more general operating range.
3) A DOB is integrated into the AMPC, which allows a comprehensive consideration of all the parameter uncertainties.

The rest of this article is arranged as follows. The converter analysis and modeling are presented in Section II. The proposed adaptive model predictive controller with the parameter update mechanism and DOB is presented in Section III. To validate the effectiveness of the proposed MPC method, the simulation and experimental results are presented in Section IV and Section V. The conclusion is drawn in Section VI.

II. Converter Topology and Modeling

A two-phase interleaved boost converter (TIBC) is applied to verify the feasibility and effectiveness of the proposed method, as shown in Fig. 1. L_1, L_2 are the inductors, C is the capacitor, Q_1, Q_2 are the power switches, D_1, D_2 are the diodes, R_L is the equivalent resistor, and δ_1, δ_2 are the gate signals generated by the pulsewidth modulation (PWM) blocks. Besides, v_{in} is the input voltage, v_o is the output voltage, i_{L1}, i_{L2} are the inductor currents, and i_o is the load current.

For modularity design, the circuit parameters of two modules are considered to be identical

$$L_1 = L_2 \;=\; L,\; d_1 = d_2 \;=\; d \tag{1}$$

where d_1, d_2 are the duty ratios for the power switches Q_1, Q_2.

The dynamic model of TIBC is obtained as

$$L\,\frac{di_{Li}}{dt} = v_{in} - (1-d_i)\,v_o, i = 1, 2 \tag{2.a}$$

$$C\,\frac{dv_o}{dt} = (1-d_1)\,i_{L1} + (1-d_2)\,i_{L2} - \frac{v_o}{R_L}. \tag{2.b}$$

Ignoring the parasitic parameters and assuming the converter operates in continuous conduction mode. Let the derivatives in (2) be zero, the static model of TIBC is

$$\begin{cases} V_o = V_{\text{in}} \,/\, (1-D) \\ V_o = (I_{L1} + I_{L2})\;(1-D)\,R_L \end{cases} \tag{3}$$

where $V_o, V_{\text{in}}, D, I_{L1}, I_{L2}$ represent the steady-state values of the variables $v_o, v_{\text{in}}, d, i_{L1}, i_{L2}$, respectively.

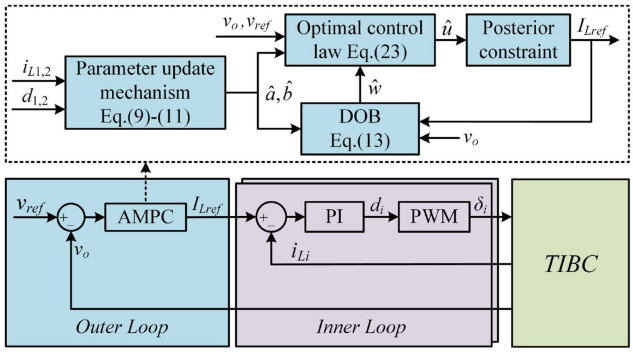

Fig. 2. Proposed control scheme for TIBC.

III. Overall Control Strategy

A. Model Conversion and Configuration

1) Cascade Control Scheme: The cascade control scheme for boost converters is shown in Fig. 2. The outer loop regulates the output voltage and generates the reference inductor current for inner loop. The inner loop regulates the inductor current to the reference value and generates duty ratios for PWM blocks. This article focuses on the voltage controller, and the PI algorithm is applied to the inner loop. Since the inner loop generally has a larger bandwidth than the outer loop, the tracking performance of the inner loop is assumed to be ideal. Then according to (2), the input-output relationship between the output voltage and inductor current is

$$Cv_o \frac{dv_o}{dt} = (i_{L1} + i_{L2})(v_{\text{in}} - L \cdot dI_{L\text{ref}}/dt) - v_o^2/R_L. \quad (4)$$

Note that the voltage dynamics (4) is the nonlinear form, thus the nonlinearity and unstable behavior requires an efficient and fast stabilizing control. However, the nonlinear model will lead to a nonlinear MPC, hence the optimization problem requires to be solved online, which will increase the computational burden of the microprocessor. And the computation time for finding the control input will also restrict the sampling rate, thus affecting the transient performance of the converter.

To develop a linear MPC method to reduce the computational burden, the voltage dynamics (4) is first linearized by the small-signal modeling method. Let the derivative in (4) be zero, the equilibrium point is

$$I_{L1,2} = I_{L\text{ref}} = v_o^2 / (2v_{\text{in}}R_L). \quad (5)$$

Linearizing (4) around the equilibrium point (5) gives

$$CV_o \frac{d\tilde{v}_o}{dt} = 2\left(I_{L\text{ref}}\tilde{v}_{\text{in}} - LI_{L\text{ref}}\frac{d\tilde{i}_{L\text{ref}}}{dt} + V_{\text{in}}\tilde{i}_{L\text{ref}}\right) - \frac{2V_o\tilde{v}_o}{R_L} \quad (6)$$

where $\tilde{v}_o$, $\tilde{v}_{\text{in}}$, and $\tilde{i}_L$ are the small-signal disturbance values.

According to (6), the control-to-output transfer function of the voltage loop is

$$G_{vi}(s) = \frac{V_o(s)}{I_{L\text{ref}}(s)} \mid_{\tilde{v}_{\text{in}}=0} = \frac{b - cs}{s + a} \quad (7)$$

where $a = \frac{2}{R_L C}$, $b = \frac{2V_{\text{in}}}{CV_o}$, and $c = \frac{LV_o}{R_L C V_{\text{in}}}$.

Denoting $u = I_{L\text{ref}}$, $y = v_o$, and the equivalent control plant for the voltage loop is reformulated as

$$\dot{y} = -ay + bu + w \quad (8)$$

where w is defined as the lumped disturbance, and the DOB is designed later to estimate its value.

2) Parameter Update Mechanism: Note that the control plant (8) is obtained by the linearization of the nonlinear system (4), it can only describe the converter dynamics near the equilibrium point (5). The values of a and b are influenced by the operating point, and some external disturbances can lead the converter to operate far from the nominal operating point. But for the typical DOB-based AMPC method, the nominal values of a, b are utilized and all the system uncertainties are estimated by the observer. In this case, if we ignore the observer dynamics, the unconstrained solution of the optimization problem derived from (8) will be a time-invariant state feedback control law, and the corresponding control gains are constant values calculated from the weighting factors and nominal model parameters a, b. Although the DOBs can provide integral actions to remove the prediction errors, the fixed control gains are only locally optimized near the nominal operation point [26], and the control performance may be degraded at other operating points.

To accurately describe the converter dynamics and guarantee the optimized control performance in the wide operating range, a parameter update mechanism is developed based on the static model (3), which utilizes the inductor currents and duty ratios to estimate the actual values of model parameters a and b. The core idea of the parameter update mechanism is to continuously linearize the voltage dynamics around its actual operating point. Since the changes in inductance and capacitance are small, only the influence of load variations and open-circuit fault on model parameters is considered, and the adverse effects caused by the other parasitic parameters will be estimated by the DOB designed in Section III-B.

According to (7), the parameter a is inversely proportional to the equivalent load resistor R_L. During the operation of TIBC, the actual value of a varies with the load power in a wide range. According to the static model (3), replacing the load resistor R_L with measured values of output voltage and inductor current, a can be approximated by

$$\hat{a} = \frac{2}{R_L C} = \frac{2(I_{L1} + I_{L2})(1 - D)}{CV_o} \approx \frac{2i_{L1}(1 - d_1) + 2i_{L2}(1 - d_2)}{Cv_o}. \quad (9)$$

The load variation will also affect parameter b. The value of b is proportional to v_{in}, which is mainly affected by the load power in most renewable energy sources. Besides, suppose that a single-phase open-circuit fault occurs, the equilibrium points of TIBC in (5) will switch to

$$i_{Li} = 0,\ i_{Lj} = I_{L\text{ref}} = v_o^2 / (v_{\text{in}}R_L),\ i, j = 1, 2,\ i \neq j. \quad (10)$$

In this case, the nominal value of b in (7) can be obtained as $b = V_{\text{in}}/(CV_o)$, which is half of the original value. Based on

the static model (3), the parameter b is approximated by

$$\hat{b} = \frac{2V_{\text{in}}}{CV_o} \approx \frac{2\,(1-D)}{C} \approx \frac{(1-d_1)+(1-d_2)}{C}. \tag{11}$$

As the saturation on the duty ratio is $[0,1]$, $(1-d_1)$ or $(1-d_2)$ will be equal to zero when a single-phase open-circuit fault occurs. The estimation of $\hat{a}$ in (9) is still valid for the fault mode, since the inductor current of the faultless circuit will rise to meet the load demand. In this process, the value of $\hat{a}$ can be adapted to the converter dynamics automatically, thus guaranteeing the relative accuracy of the system model.

B. Design of the Disturbance Observer

According to the analysis in Section III-A, the impact of load variations and open-circuit faults on the system dynamics is not infinite. Assume the derivatives of lumped disturbances in (8) are bounded and satisfy [27]

$$\|\dot{w}\| < \infty, \lim_{t\to\infty} \dot{w} = 0. \tag{12}$$

Substituting the estimated values of $\hat{a}$ and $\hat{b}$ into (8), and the DOB is given as

$$\dot{\hat{w}} = -L_0\left[\hat{w} - \hat{a}y + \hat{b}u\right] + L_0\dot{y} \tag{13}$$

where $\hat{w}$ is the estimated value of w, and L_0 is the observer gain.

Define the estimation error as $e_r = w - \hat{w}$, and combine (8) and (13), the derivative of e_r is

$$\dot{e}_r = -L_0 e_r + \dot{w}. \tag{14}$$

Therefore, the estimation error e_r is bounded and its bounds are related to $\dot{w}$. With the assumption that $\dot{w} = 0$ as $t \to \infty$, the estimation error e_r is asymptotically stable.

C. Adaptive Predictive Controller Design

In this article, the closed-form MPC developed in [28] is used to obtain the optimal control law. For power converters, the cost function can be defined as

$$J = \frac{1}{2}\int_0^{T_s}\left\{Q[y_r(t+\tau) - y_p(t+\tau)]^2 + R[u_c(t) - u_r(t)]^2\right\}d\tau \tag{15}$$

where y_{ref} and $y_p(t+\tau)$ are the reference value and predicted value of the output voltage, respectively. $u(t)$ and $u_r(t)$ are the future control input and the desired control input, respectively. T_s is the prediction time, and Q, R are the weighting factors.

In (15), the predicted voltage $y_p(t+\tau)$ should be expanded into the $(\rho+r)th$ order Taylor series expansion. ρ is the input relative degree and r is the control order. The control order r is selected to describe the variation of the control input within the prediction time and ensure the closed-loop stability [28]. Since the input relative degree of the plant (8) is one, the control order is selected as one in this article. Then, the control sequence within the prediction time is defined as $\bar{u}(t) = [u(t), \dot{u}(t)]^T$, and the predicted output voltage is expressed as

$$y_p(t+\tau) = [\Gamma_1(\tau), \Gamma_2(\tau)]\begin{bmatrix} Y_1(t) \\ Y_2(t)\end{bmatrix} \tag{16}$$

where $\Gamma_1(\tau) = 1, \Gamma_2(\tau) = [\tau, 0.5\tau^2]$, $Y_1(t) = y(t)$, and $Y_2(t) = [\dot{y}(t), \ddot{y}(t)]^T$.

In order to enhance the prediction accuracy and eliminate steady-state errors, the disturbance estimations $\hat{w}$ are utilized to correct the output predictions. Hence the derivatives in (16) can be expressed in the matrix form as

$$Y_2(t) = Y_w(t) + W_a\bar{u}(t) \tag{17}$$

where $Y_w(t) = Y(t) + W_b d(t), Y(t) = [-\hat{a}y(t), \hat{a}^2 y(t)]^T$

$$W_a = \begin{bmatrix} \hat{b} & 0 \\ -\hat{a}\hat{b} & \hat{b}\end{bmatrix}, W_b = \begin{bmatrix} 1 & 0 \\ -\hat{a} & 1\end{bmatrix}, d(t) = [\hat{w}, 0]^T.$$

Define the reference values corresponding to $Y_1(t)$ and $Y_2(t)$ as $Y_{c1}(t)$ and $Y_{c2}(t)$ respectively. The future reference voltage $y_r(t+\tau)$ within the prediction time can be obtained in a similar way as (16). And define $\bar{u}_r(t) = [u_r(t), \dot{u}_r(t)]^T$ as the desired control sequence, by substituting the desired condition $Y_2(t) = Y_{c2}(t)$ into (17), the $\bar{u}_r(t)$ is obtained as

$$\bar{u}_r(t) = W_a^{-1}\left[Y_{c2}(t) - Y_w(t)\right]. \tag{18}$$

The future control input $u_c(t)$ and the desired control input $u_r(t)$ in (15) is expressed as

$$u_c(t) = \Gamma_r(\tau)\,\bar{u}(t), u_r(t) = \Gamma_r(\tau)\,\bar{u}_r(t) \tag{19}$$

where $\Gamma_r(\tau) = [1, \tau]^T$.

Combining (16) and (19), the performance index in (15) can be formulated as

$$\begin{aligned} J &= \tfrac{1}{2}\int_0^{T_s}\Big\{\left[(Y_1 - Y_{c1})^T, (Y_2 - Y_{c2})^T\right]\begin{bmatrix}\Gamma_1^T \\ \Gamma_2^T\end{bmatrix} \\ &\times Q[\Gamma_1, \Gamma_2]\begin{bmatrix} Y_1 - Y_{c1} \\ Y_2 - Y_{c2}\end{bmatrix} + (\bar{u} - \bar{u}_r)^T\Gamma_r^T R\Gamma_r(\bar{u} - \bar{u}_r)\Big\}d\tau \\ &= (Y_1 - Y_{c1})^T\xi_1(Y_1 - Y_{c1}) + 2(Y_1 - Y_{c1})^T\xi_2(Y_2 - Y_{c2}) \\ &+ (Y_2 - Y_{c2})^T\xi_3(Y_2 - Y_{c2}) + (\bar{u} - \bar{u}_r)^T\xi_4(\bar{u} - \bar{u}_r) \end{aligned} \tag{20}$$

where

$$\xi_1 = \frac{1}{2}\int_0^{T_s}\Gamma_1^T Q\Gamma_1 d\tau = \frac{Q}{2}T_s,$$

$$\xi_2 = \frac{1}{2}\int_0^{T_s}\Gamma_1^T Q\Gamma_2 d\tau = \frac{Q}{2}\begin{bmatrix}\frac{T_s^2}{2} & \frac{T_s^3}{6}\end{bmatrix}$$

$$\xi_3 = \frac{1}{2}\int_0^{T_s}\Gamma_2^T Q\Gamma_2 d\tau = \frac{Q}{2}\begin{bmatrix}\frac{T_s^3}{3} & \frac{T_s^4}{8} \\ \frac{T_s^4}{8} & \frac{T_s^5}{20}\end{bmatrix}$$

$$\xi_4 = \frac{1}{2}\int_0^{T_s}\Gamma_r^T R\Gamma_r d\tau = \frac{R}{2}\begin{bmatrix}T_s & \frac{T_s^2}{2} \\ \frac{T_s^2}{2} & \frac{T_s^3}{3}\end{bmatrix}.$$

The derivative of the cost function with respect to $\bar{u}$ gives

$$\begin{aligned} \partial J/\partial\bar{u} = {} & 2\left(W_a^T\xi_3 W_a + \xi_4\right)\bar{u} + 2W_a^T\xi_2^T(Y_1 - Y_{c1}) \\ & - 2\xi_4^T\bar{u}_r + 2W_a^T\xi_3^T[Y_w - Y_{c2}]. \end{aligned} \tag{21}$$

Letting $\partial J/\partial \bar{u} = 0$ and combining (18), the solution of the optimization problem (20) is

$$\bar{u} = -\left(\xi_3 W_a + W_a^{-T}\xi_4\right)^{-1}\xi_2^T\left(Y_1 - Y_{c1}\right) - W_a^{-1}\left(Y_w - Y_{c2}\right). \tag{22}$$

Taking the first row of $\bar{u}^*$, the unconstrained optimal control law $\hat{u}(t)$ is obtained as

$$\hat{u}\ (t) = -k_1\left(y\left(t\right) - y_{ref}\right) + k_2\left(\dot{y}_{\text{ref}} + \hat{a}y\left(t\right) - \hat{w}\right) \tag{23}$$

where k_1 is the first row of $\left(\xi_3 W_a + W_a^{-T}\xi_4\right)^{-1}\xi_2^T$, $k_2 = 1/\hat{b}$

$$k_1 = \frac{T_s\hat{b}Q\left[12Q\hat{b}^2T_s^2 - 160R\hat{a}T_s + 240R\right]}{\left(3Q^2\hat{b}^4 + 48QR\hat{a}^2\hat{b}^2\right)T_s^4 - 96QR\hat{a}\hat{b}^2T_s^3 + 104QR\hat{b}^2T_s^2 + 240R^2}.$$

Define the maximum allowable inductor current is $I_{L\max}$, the optimal control law can be obtained by introducing the posterior constraint on (23).

The overall control block diagram of AMPC cascaded with PI control is shown in Fig. 2. When load changes or open-circuit faults occur, although they cannot be predicted in advance, the parameter update mechanism (9)–(11) can still identify the real values of model parameters at the new operating point through the changing inductor current and duty ratio. Then, the estimated values $\hat{a}$, $\hat{b}$ will be transmitted to the DOB (13) and control law (23). Based on the adaptive model, the observer will calculate the total error between the control plant and the practical system. Then, the control law will calculate the optimal control gains k_1, k_2 for the current operating point and generate the unconstrained control input. After *a posterior* constraint, the reference inductor current is sent to the inner loop PI control to generate the duty ratios.

D. Stability Analysis

The stability of the proposed AMPC law is established by the following theorem.

Remark 1: For the prediction time $T_s \le 3/(2\hat{a})$, the control gain $k_1 > 0$ always holds; for the prediction time $T_s > 3/(2\hat{a})$, the condition for $k_1 > 0$ is $R/Q < (3\hat{b}^2T_s^2)/(40\hat{a}T_s - 60)$.

Theorem 1: Suppose that the lumped disturbance satisfies the boundary conditions provided in (12), and the weighting factors are selected as Remark 1, then the closed-loop control system is asymptotic stable.

The proof of Remark 1 and Theorem 1 is given in Appendix.

Moreover, to better illustrate the impact of parameter update mechanism on the control performance, assuming the converter operates at a nonrated point, the plant (8) is rewritten as

$$\dot{y} = -a_1 y + b_1 u + w \tag{24}$$

where a_1, b_1 are obtained based on the current operating point.

Considering the mismatch effect of a_1, b_1, assume the model parameters used to formulate the control law are a_0, b_0, then the optimal control law in (23) can be reformulated as

$$\hat{u}\ (t) = -k_1\left(y\left(t\right) - y_{\text{ref}}\right) + \left(a_0 y\left(t\right) - \hat{w}\right)/b_0 \tag{25}$$

where the time derivative of the reference value $\dot{y}_{\text{ref}}$ is omitted since it is not always available, and k_1 is of the same form as in (23) but calculated from a_0, b_0.

Applying Laplace transform into (13), the transfer function of the DOB is

$$\hat{w} = G_1\ (s)\, y\,(t) - G_2\,(s)\,\hat{u}\,(t) \tag{26}$$

where $G_1(s) = \frac{(s+a_0)L_0}{s+L_0}$, $G_2(s) = \frac{b_0L_0}{s+L_0}$.

Combining (24)–(26), the open-loop and closed-loop transfer functions of the control system are

$$G_o\ (s) = \frac{k_b b_0 k_1\left(s + L_0\right)}{s^2 + \left[\left(k_a - k_b\right)a_0 + L_0k_b\right]s} \tag{27}$$

$$\begin{aligned} G_c\ (s) &= \frac{y\,(s)}{y_r\,(s)} \\ &= \frac{k_b b_0 k_1\left(s + L_0\right)}{s^2 + \left[\left(k_a - k_b\right)a_0 + L_0k_b + k_b b_0 k_1\right]s + k_b b_0 k_1 L_0} \end{aligned} \tag{28}$$

where $k_b = b_1/b_0,\ k_a = a_1/a_0$.

To simplify the analysis, the mismatches of model parameter a_1 is analyzed first. Letting $k_b = 1$ and the characteristic equation is reformulated with respect to k_a as

$$1 + k_a\,\frac{a_0 s}{s^2 + \left(L_0 - a_0 + b_0k_1\right)s + b_0k_1L_0} = 0. \tag{29}$$

For illustration purposes, letting $a_0 = 400,\ \ b_0 = 2000,$ $L_0 = 500,\ \ k_1 = 0.25$. Then, the Bode plot of the open-loop transfer function (27) with different values of k_a is shown in Fig. 3(a). Besides, the root locus of (29) is shown in Fig. 3(b), where k_a changes from 0.25 to 4.

It can be seen from Fig. 3(a) that with the increase of k_a, the system bandwidth decreases, which leads to a slower dynamic response. However, according to Fig. 3(b), when $k_a \le 1$, two poles are complex roots, which means that there is an overshoot in the step response. Hence, making $k_a = 1$ can avoid overshoot and obtain a relatively high dynamic response.

Then, the model mismatches caused by model parameter b are discussed. Letting $k_a = 1$ and the characteristic equation with respect to k_b is reformulated as

$$1 + k_b\,\frac{\left(L_0 - a_0 + b_0k_1\right)s + b_0k_1L_0}{s^2 + a_0 s} = 0. \tag{30}$$

Making $a_0 = 400,\ b_0 = 2000,\ L_0 = 500,\ k_1 = 0.25$ and the Bode plot the open-loop transfer function of (27) with different values of k_b is shown in Fig. 4(a). Besides, the root locus of (30) is shown in Fig. 4(b), where k_b changes from 0.25 to 2.

The parameter b is determined by the circuit structure, which may decrease due to circuit fault. It can be seen from Fig. 4(a) that smaller k_b leads to smaller bandwidth. Besides, according to Fig. 4(b), when $0.44 \le k_b \le 1$, there is an overshoot in the step response. Therefore, making $k_b \ge 1$ could obtain a better control performance. However, it should be noted that the outer loop bandwidth cannot be too large to avoid measurement noise. Besides, it is generally lower than the observer bandwidth.

For the proposed AMPC method, since a parameter update mechanism is utilized to estimate the actual values of a, b in (8) in real-time, the condition $k_a \approx 1, k_b \approx 1$ always holds, hence it can guarantee the desired control performance in a wide range.

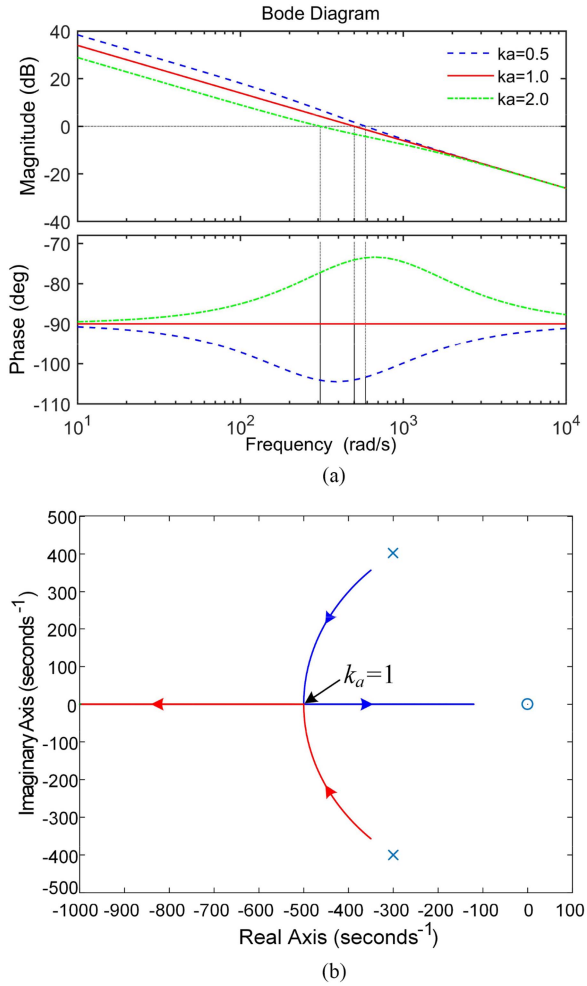

Fig. 3. Influence of the variation of k_a on control performance.

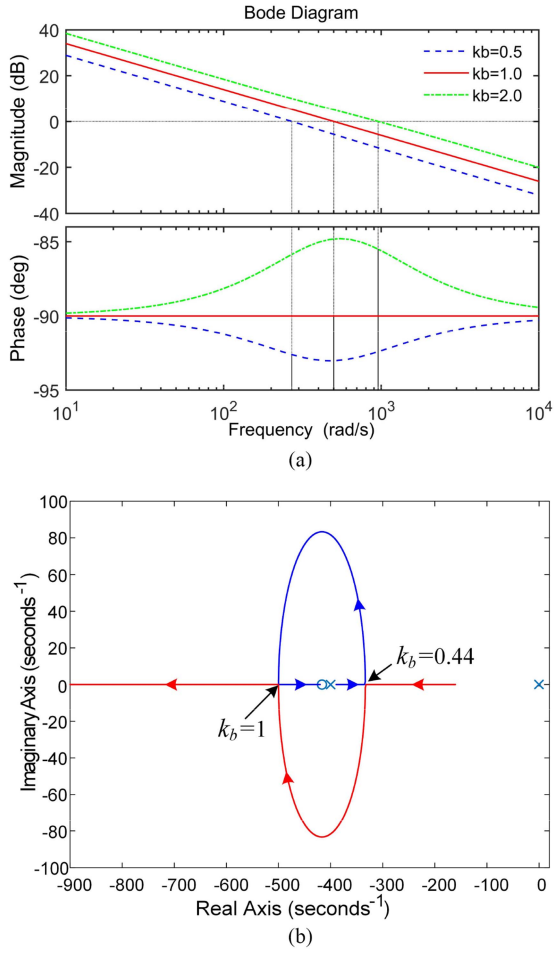

Fig. 4. Influence of the variation of k_b on control performance.

Moreover, substitute $k_a = 1$, $k_b = 1$ into (28) and replace b_1 with its estimated value $\hat{b}$, the closed-loop transfer function is

$$G_c(s) = \frac{y(s)}{y_r(s)} = \frac{\hat{b}k_1}{s + \hat{b}k_1}. \tag{31}$$

To simplify the analysis, suppose the weight ratio is tuned as $R/Q = 0$, and we only focus on eliminating the tracking errors. Then a simpler version of k_1 in (23) is derived as $k_1 = 4/(\hat{b}T_s)$. This indicates that the system bandwidth $\hat{b}k_1$ is a constant value, which is only determined by the prediction time T_s, and changes in model parameters a, b will not affect the system dynamics.

In addition, the transfer function from disturbance to system output can be obtained from (24) to (26) as

$$G_c(s) = \frac{y(s)}{w(s)} = \frac{s}{s^2 + \left(L_0 + \hat{b}k_1\right)s + \hat{b}k_1 L_0}. \tag{32}$$

For illustration purposes, letting $\hat{b} = 2000$, $k_1 = 0.25$. Then, the Bode plot of (32) with different L_0 is given in Fig. 5. It can be seen that a larger L_0 leads to stronger robustness, due to the disturbance of TIBC is generally low frequency, but the upper limit of L_0 is limited by the sampling rate and sensor noise.

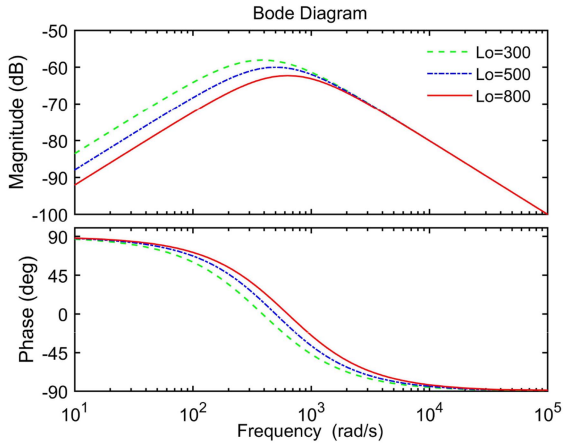

Fig. 5. Influence of L_0 on the antidisturbance performance.

IV. Simulation Results

To validate the theoretical analysis, the converter model with the proposed method is built and tested in MATLAB\Simulink. The circuit parameters of the converter are given in Table I. The

TABLE I
CIRCUIT PARAMETERS OF TIBC

Variables	Description	Nominal Value
v_o	Output voltage	48 V
v_{in}	Input voltage	16-24 V
L_1, L_2	Nominal inductance	200 μH
C	Nominal capacitance	470 μF
P	Nominal power	250 W
f_s	Switching frequency	50 kHz

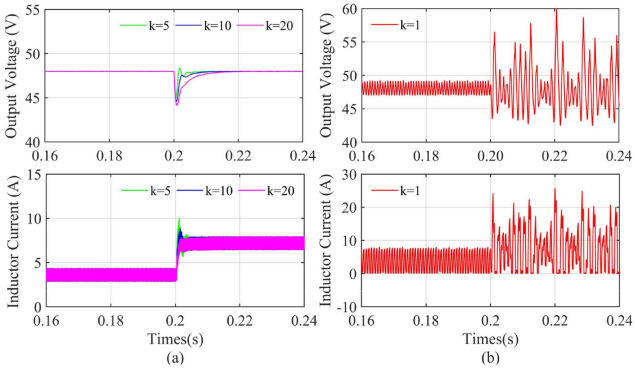

Fig. 6. Simulation results of the converter under different k.

sampling rates of the inductor current and output voltage are 50 and 2.5 kHz, respectively. The control parameters for the inner loop PI algorithm are tuned as $k_{p1} = 0.05$, $k_{i1} = 30$.

For the proposed controller, the average filters are utilized to smooth the estimated values $\hat{a}$ and $\hat{b}$. All the inductor currents and duty ratios used in the parameter update mechanism (9) and (11) take an average value at every 20 sampled values. And the maximum reference inductor current $I_{L\max}$ is 15 A.

A. System Verification

The selection of prediction time T_s and weight ratio R/Q will be discussed in this section.

First, the prediction time T_s is designed, and the weight ratio is set at zero for simplicity. According to (31), the bandwidth of the closed-loop system is $\omega_c = 4/T_s$. Thus, a smaller prediction time is helpful to improve dynamic response, but decreases the noise immunity. The lower limit of T_s is restricted by the sampling period T_f, since AMPC is implemented based on the prediction of future converter behavior. Define $k = T_s/T_f$, and the dynamic responses with different values of k are presented in Fig. 6, where the load current steps from 3.5 to 7 A at 0.2 s.

As can be seen, when $k = 1$, too short prediction time leads to large static errors, and when the load current steps, there are severe oscillations. When k varies from 5 to 20, larger k leads to longer recovery time, which is consistent with the analysis above. Thus, the prediction time is chosen to be 10 times of the sampling time in this article.

The weight ratio is used to penalize the control variation and guarantee system stability. When the prediction time is tuned as 4 ms, the dynamic response of the system under different weight ratios is shown in Fig. 7(a), where the load current steps from 3.5 to 7 A at 0.2 s.

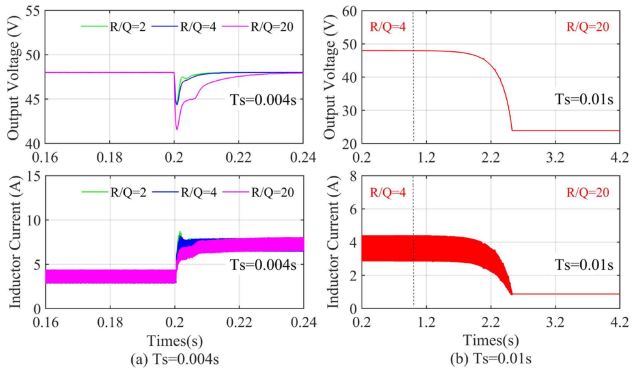

Fig. 7. Simulation results of the converter under different R/Q.

According to (7), when the load current is 3.5 A, $a = 310$, $b = 2000$. Then, the inequality $T_s \leq 3/(2\hat{a})$ in Remark 1 holds and the system stability is independent of the weight ratio. As can be seen in Fig. 7(a), all AMPCs with different weight ratios can regulate the output voltage to the reference value. Besides, larger R/Q leads to smaller current overshoot but larger voltage drops and longer recovery time. Thus, the weight ratio is chosen as 4 to balance control variations and dynamic response.

For illustration purposes, the prediction time is tuned as 0.01s so that $T_s > 3/(2\hat{a})$. According to Remark 1, the upper limit of the weight ratio is derived as 18.7 when the load current is 3.5A. The dynamic response of the converter is shown in Fig. 7(b), where the weight ratio changes from 4 to 20 at 1s.

As can be observed from Fig. 7(b), when the weight ratio is 4, the output voltage can converge to the reference value. When the weight ratio changes to 20, the system becomes unstable and the output voltage drops to 24V, which is consistent with the analysis in Remark 1 and Theorem 1. The negative control gain k_1 makes the control input negative, which in turn makes the duty ratios of the system reach the lower limit of 0.

B. Simulation Comparison

To evaluate the dynamic performance of the AMPC method, it is compared with the adaptive model based-MPC (AM-MPC) for the case of load variations and open-circuit faults. The AM-MPC is implemented according to [29], which has a DOB and an optimized voltage change rate $\tilde{b}$ calculated by the steepest descent algorithm. The control parameters of the AM-MPC method are set as $a = 450$, $T_s = 3$ ms, $R/Q = 4$, and the optimized coefficients are $\lambda = 0.25$, $\mu = 1$.

Fig. 8 shows the simulation results of TIBC under step load disturbance. The load current steps from 3.5 to 7 A at 0.25 s and steps back to 3.5 A at 0.35 s. It can be observed from Fig. 8 that both the AMPC and AM-MPC controllers can remove the offset caused by load changes. For the AM-MPC controller, the model parameter b varies with the load current. For the AMPC controller, a smaller voltage drop/rise and shorter recovery time are obtained. As the load current changes, the model parameter a steps from 328 to 656 and steps back to 328 at 0.35 s. This is consistent with the analysis in Section III. Since the constant

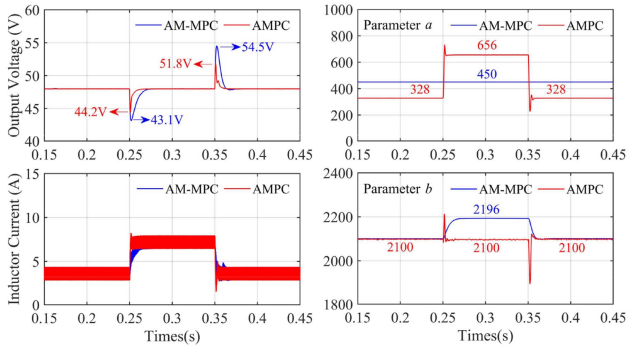

Fig. 8. Simulation results of AM-MPC and AMPC methods under step load disturbance.

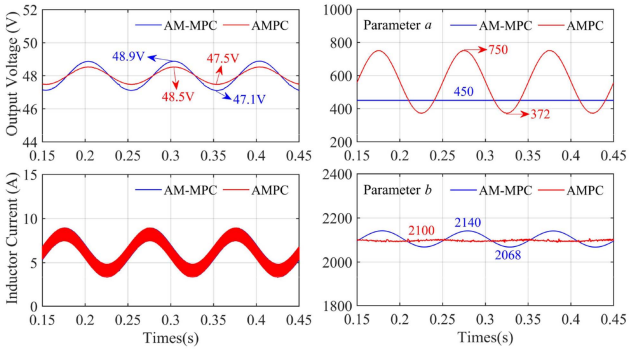

Fig. 9. Simulation results of AM-MPC and AMPC methods under sinusoidal load disturbance.

voltage source is applied in the simulation, the model parameter b remains unchanged after the fluctuation.

The simulation results of two controllers under time-varying load disturbance are shown in Fig. 9. The load current is set to $i_o = 6 + 2\sin(20\pi t)A$. It can be observed from Fig. 9 that the AMPC controller still shows a better dynamic performance, the voltage fluctuations of AMPC are smaller than the AM-MPC. For the AM-MPC controller, parameter b changes with load current. For the AMPC controller, when the load current varies sinusoidally, the model parameter a varies from 372 to 750, and b remains unchanged, which is consistent with the theoretical analysis in Section III.

Assume the second phase circuit of TIBC has an open-circuit fault, and the simulation results are presented in Fig. 10. It can be observed from Fig. 10 that when the open-circuit fault occurs at 0.2 s, the inductor current of the fault phase drops to zero, and the inductor current of the healthy phase gradually rises to meet the load power. For the AMPC controller, the model parameter a becomes larger after the fluctuation, this is because when the open-circuit fault occurs, the system efficiency is reduced and a larger inductor current is required to match the load. Besides, the model parameter b gradually decreases from 2100 to 1160, which is consistent with the analysis in Section III. For the AM-MPC controller, the model parameter b also changes from 2100 to 1560. However, as can be observed, in the transient process, the AMPC controller still has a smaller voltage drop and shorter recovery time than AM-MPC.

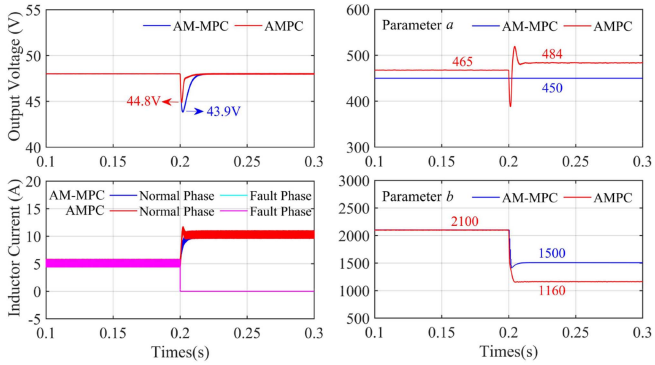

Fig. 10. Simulation results of AM-MPC and AMPC methods under open-circuit fault.

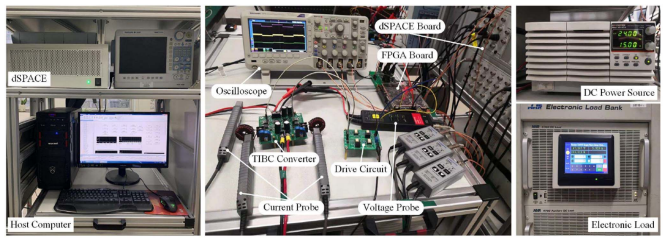

Fig. 11. Experimental setup.

TABLE II
PARAMETERS OF THREE CONTROLLERS

Controller	Outer Loop	Inner loop
AMPC	$T_s = 4$ ms, $R/Q = 4, L_0 = 500$	$k_p = 0.05, k_i = 30$
AM-MPC	$a_0 = 450, T_s = 3$ ms, $R/Q = 4$ $L_0 = 500, \lambda = 0.25, \mu = 1$	
IMPC	$a_0 = 450, b_0 = 2000$ $T_s = 3$ ms, $R/Q = 2, k_I = 80$	

V. EXPERIMENTAL RESULTS

The experimental setup is presented in Fig. 11. It consists of a dc power supply, a TIBC, a dSPACE DS1007, an FPGA board, and an electronic load. The controller is implemented in dSPACE platform to generate the control signals, and the FPGA board is used to realize the phase shift. The circuit parameters and sampling rates of the converter are the same as that in Section IV.

In experimental tests, to further evaluate the effectiveness of the proposed AMPC method, the AM-MPC method and MPC with integrator (IMPC) are chosen as benchmarks in subsequent tests. The AM-MPC is realized according to [29], which utilizes a DOB to estimate unknown terms and uses the steepest descent method to update the optimized change rate $\tilde{b}$. The IMPC uses an integral variable to account for disturbance terms.

Since this article mainly focuses on the robustness to the large external disturbance, to avoid the influence of parameter tuning and enable a fair comparison, the three controllers are tuned to perform similar tracking performance. The parameters of the three controllers are given in Table II, and their tracking performances are shown in Fig. 12, where the reference voltage steps from 48 to 56 V and then steps back to 48 V. It can be

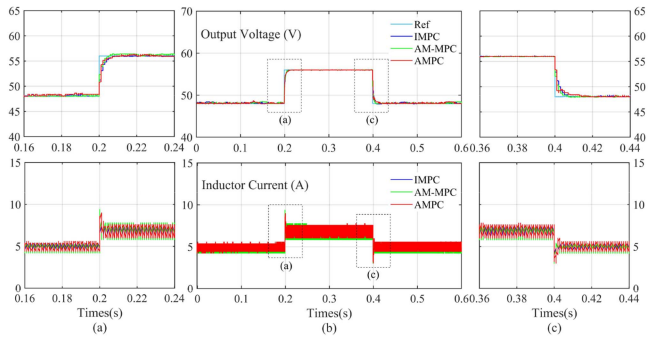

Fig. 12. Tracking performance of three controllers.

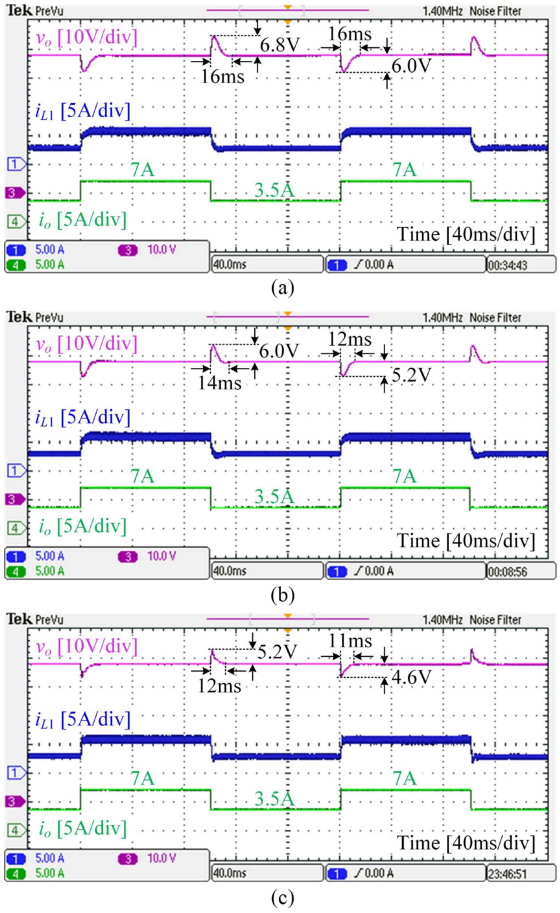

Fig. 13. Experimental results of TIBC under step load changes.

seen from Fig. 12 that all three controllers exhibit similar and satisfactory tracking performance. Then, the robustness of the three controllers will be compared under external disturbances.

A. Case I: Step Load Disturbance

The robustness of controllers against step load disturbance is tested in this part. The load current is set to change between 7 and 3.5 A periodically. The experimental results of TIBC under different controllers are shown in Fig. 13.

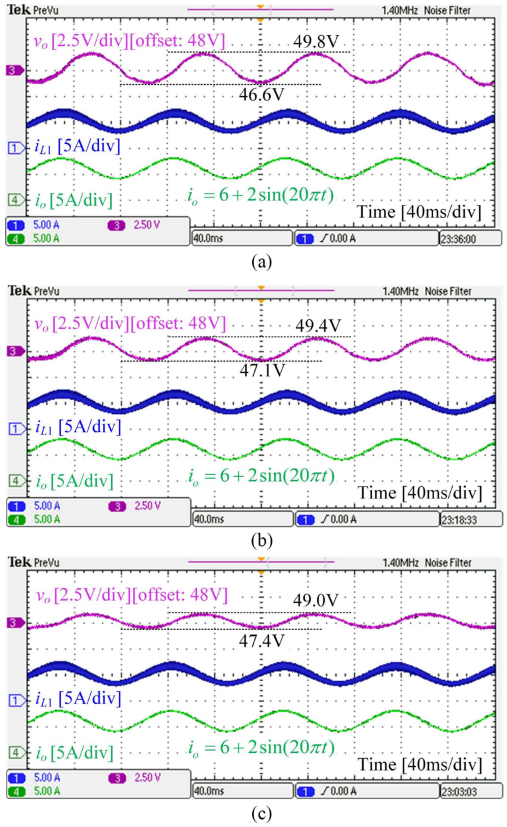

Fig. 14. Experimental results of converter under sinusoidal load disturbance.

It can be seen from Fig. 13 that when the load current steps, the output voltage will deviate from the reference value. All the three controllers can regulate the output voltage to the reference value after load changes. But among these three controllers, the proposed AMPC controller shows the smallest voltage drop/rise and the shortest recovery time. Therefore, the AMPC controller shows the strongest robustness against step load disturbance.

B. Case II: Time-Varying Load Disturbance

To test the robustness of controllers against the time-varying disturbance, the load current is set to $i_o = 6 + 2\sin(20\pi t)A$. The experimental results of TIBC are shown in Fig. 14.

It can be seen from Fig. 14 that when the load current changes sinusoidally, the output voltage also varies with the load current. For the IMPC controller, the output voltage varies from 46.6 to 49.8 V. For the AM-MPC controller, the output voltage varies from 47.1 to 49.4 V. However, for the AMPC controller, the output voltage only varies from 47.4 to 49 V. The proposed method exhibits the strongest robustness against time-varying load disturbance.

C. Case III: Hardware Open-Circuit Fault

The robustness of controllers against hardware open-circuit fault is tested. Assume the second phase circuit of the converter has an open-circuit fault, and the experimental results of TIBC are shown in Fig. 15.

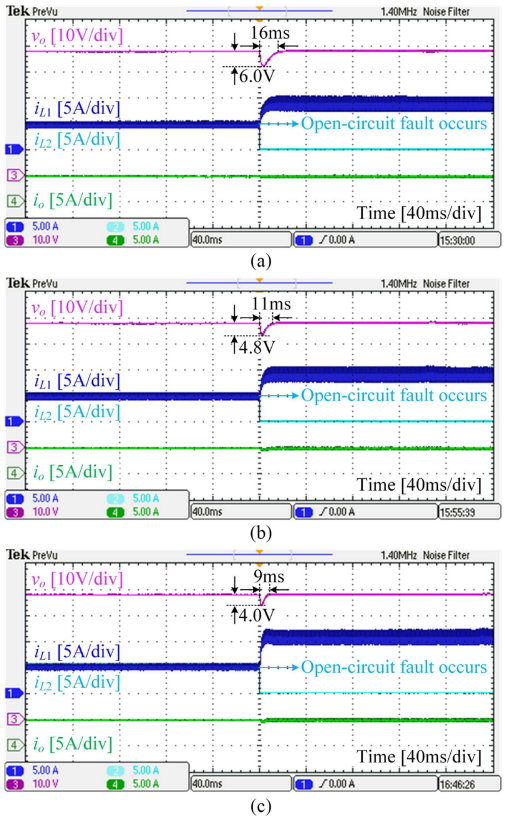

Fig. 15. Experimental results of TIBC under open-circuit fault.

As can be observed from Fig. 15, when an open-circuit fault occurs, the inductor current of the fault phase i_{L2} drops to zero, and the inductor current of the healthy phase i_{L1} gradually rises to match the load power. The healthy phase inductance takes on all the load power, leading to a larger current ripple. Since AM-MPC also contains an optimized change rate $\tilde{b}$, it has a similar control performance to AMPC, but AMPC shows the smallest voltage drop and the shortest recovery time among these three controllers. This indicates the proposed AMPC method exhibits the strongest robustness against open-circuit faults.

To quantitatively compare the control performances of three controllers, the integral of time multiplied by the absolute value of error (ITAE) and root-mean-square error (RMSE) [30] are used as performance indexes, calculated as

$$\text{ITAE} = \int_0^t t\,|y_r - y|\,d\tau\,, \text{RMSE} = \sqrt{\int_0^t \frac{1}{t}(y_r - y)^2 d\tau}\,. \tag{33}$$

The performance indexes of three controllers for the above three test cases are given in Table III. It can be observed from Table III that the proposed AMPC method has an obvious performance improvement for power converters. Specifically, for Case I, compared with AM-MPC, the ITAE and RMSE of AMPC are reduced by 36.2% and 52.7%. For case II, compared with AM-MPC, the ITAE and RMSE of AMPC are reduced by 35.7% and 55.9%. For case III, compared with AM-MPC, the ITAE and RMSE of AMPC are reduced by 27.4% and 42.2%.

TABLE III
QUANTITATIVE PERFORMANCE COMPARISON OF THREE CONTROLLERS

Test Type	Controller	ITAE	RMSE
Case I	IMPC	0.6173	1.2015
	AM-MPC	0.4721	0.7292
	AMPC	0.3013	0.3445
Case II	IMPC	1.3972	0.7439
	AM-MPC	1.0505	0.4313
	AMPC	0.6754	0.1904
Case III	IMPC	0.1660	0.1231
	AM-MPC	0.1097	0.0545
	AMPC	0.0796	0.0315

TABLE IV
EXECUTION TIME OF DIFFERENT ADAPTIVE MPC METHODS

Task	AMPC	IMPC	AM-MPC	RLS-AMPC
Parameter Update	3.26μs	0μs	3.57μs	18.79μs
MPC Control Law	5.29μs	3.69μs	5.29μs	3.58μs
Total Time	8.55μs	3.69μs	8.86μs	22.37μs

To evaluate the computational burden of the AMPC method, the execution time is compared with IMPC, AM-MPC, and the RLSs-based AMPC (RLS-AMPC) in [22]. All four controllers are implemented for the TIBC on DSP28335 (150 MHz). The execution time of the parameter update module and predictive control law is given in Table IV.

As can be observed from Table IV, the execution time of the proposed parameter update mechanism is shorter than those of the AM-MPC and RLS-AMPC. Since an additional DOB is utilized in AMPC and AM-MPC, the execution time of the predictive control law is larger than that of RLS-AMPC. The total execution time of AMPC is shorter than that of AM-MPC and RLS-MPC, but larger than that of IMPC since IMPC has a simple structure. However, the increase in execution time is acceptable considering the improved control performance.

D. Stability Verification

As can be observed from the previous experiments in cases I– III, when the prediction time is selected as $T_s = 4$ ms, the system can converge to the reference value since the inequality $T_s \leq 3/(2\hat{a})$ in Remark 1 holds.

In this part, the load resistance is set to 13.7Ω, and according to (7), $a = 310, b = 2000$. The prediction time is selected as 0.01s to satisfy $T_s > 3/(2\hat{a})$. According to Remark 1, the upper limit of the weight ratio is derived as 18.7. The experimental results of the proposed method with $T_s = 0.01s$ are presented in Fig. 16, where the weight ratio changes from 4 to 20.

As can be observed from Fig. 16, when the weight ratio is 4, the output voltage can be regulated to 48 V, and the duty ratio is slightly higher than 0.5 due to the effect of parasitic parameters. When the weight ratio R/Q changes to 20, the system becomes unstable, the output voltage drops to 24V, and the duty ratios of PWM blocks drop to 0.

Therefore, the experimental results agree with the simulation results, which demonstrates the stability analysis in Section III.

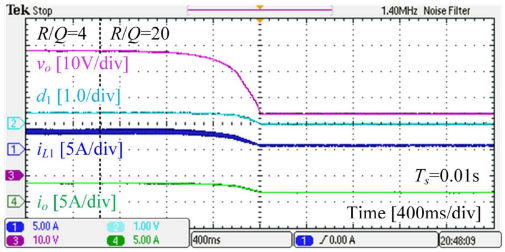

Fig. 16. Experimental results of the AMPC with $T_s = 0.01$ s.

VI. Conclusion

To mitigate model mismatches and enhance the robustness to disturbances, an AMPC method is developed for an interleaved boost converter. The adaptive predictive model is updated at each sampling period using a parameter update mechanism and a DOB. Hence, the proposed method is adaptive to the current operating point. An explicit control law is derived by solving the optimization problem offline, which helps reduce the computational burden of the microprocessor.

The simulation and experimental studies are conducted in the laboratory. The results indicate that compared with the IMPC and AM-MPC methods, the control performance of the AMPC method has been improved significantly. The ITAE and RMSE of AMPC are reduced by 35.7% and 52.7% under load changes, and the ITAE and RMSE of AMPC are reduced by 27.4% and 42.2% when an open-circuit fault occurs. Besides, the execution time of the AMPC method on DSP28335 (150 MHz) is 8.55μs, which is acceptable for the studied converter with a sampling period of 0.4 ms.

Appendix

A. Remark 1

For k_1, the sign of its numerator is determined by

$$N_u = 12Q\hat{b}^2T_s^2 - 160R\hat{a}T_s + 240R. \tag{A.1}$$

In this case, N_u can be considered as a quadratic function of prediction time T_s, and the condition for $N_u > 0$ with any T_s is obtained as

$$R/Q < 9\hat{b}^2/\left(20\hat{a}^2\right). \tag{A.2}$$

For simplicity, define $a_T = \hat{a}\,T_s,\ b_T = \hat{b}\,T_s$. The denominator of k_1 can be expressed as

$$D_e = 3Q^2b_T^4 + 48QRa_T^2b_T^2 - 96QRa_Tb_T^2 + 104QRb_T^2 + 240R^2. \tag{A.3}$$

Then, the following inequality holds

$$D_e > f\left(a_T\right) = QRb_T^2\left(48a_T^2 - 96a_T + 104\right). \tag{A.4}$$

Hence, $f(a_T)$ is a quadratic function of a_T, and its minimum value is always greater than zero. Therefore, when the condition in (A.3) is satisfied, the control gain k_1 is always positive.

It is worth noting that (A.2) is a sufficient condition for $k_1 > 0$, which can ensure the control gain k_1 is positive for any prediction time T_s. However, for a given prediction time T_0, the range of R/Q for $k_1 > 0$ will be larger than (A.2).

Substitute T_0 into (A.1), it can be rewritten as

$$N_u = 12Q\hat{b}^2T_0^2 + (240 - 160\hat{a}T_0)\,R. \tag{A.5}$$

According to (A.4)-(A.5), for $T_0 \le 3/(2\hat{a})$, $k_1 > 0$ always holds; for $T_0 > 3/(2\hat{a})$, the necessary and sufficient condition for $k_1 > 0$ is

$$R/Q < \frac{3\hat{b}^2T_0^2}{20\left(2\hat{a}T_0 - 3\right)}. \tag{A.6}$$

B. Theorem 1

Define the voltage tracking error as $e_v = y(t) - y_{ref}$, and combine (8), (14), and (23), the closed-loop error system is

$$\dot{E}_{v,r} = A_\varepsilon\,E_{v,r} + B_\varepsilon\dot{w} \tag{A.7}$$

where $E_{v,r} = [e_v, e_r]^T$, $A_\varepsilon = \begin{bmatrix} -\hat{b}k_1 & 1 \\ 0 & -L_0 \end{bmatrix}$, $B_\varepsilon = [0,1]^T$.

Since A_ε is Hurwitz stable, the error system (A.7) is bounded and its bound depends on $\dot{w}$. With the assumption that $\dot{w} = 0$ as $t \to \infty$, the error system is asymptotically stable.

References

[1] O. Hegazy, J. V. Mierlo, and P. Lataire, "Analysis, modeling, and implementation of a multidevice interleaved DC/DC converter for fuel cell hybrid electric vehicles," *IEEE Trans. Power Electron.*, vol. 27, no. 11, pp. 4445–4458, Nov. 2012.

[2] Q. Xu, W. Jiang, F. Blaabjerg, C. Zhang, X. Zhang, and T. Fernando, "Backstepping control for large signal stability of high boost ratio interleaved converter interfaced DC microgrids with constant power loads," *IEEE Trans. Power Electron.*, vol. 35, no. 5, pp. 5397–5407, May 2020.

[3] A. Cid-Pastor, R. Giral, J. Calvente, V. I. Utkin, and L. Martinez-Salamero, "Interleaved converters based on sliding-mode control in a ring configuration," *IEEE Trans. Circuits Syst. I, Reg. Papers*, vol. 58, no. 10, pp. 2566–2577, Oct. 2011.

[4] Y. Huangfu, Q. Li, L. Xu, R. Ma, and F. Gao, "Extended state observer based flatness control for fuel cell output series interleaved boost converter," *IEEE Trans. Ind. Appl.*, vol. 55, no. 6, pp. 6427–6437, Nov./Dec. 2019.

[5] Q. Xu, N. Vafamand, L. Chen, T. Dragičević, L. Xie, and F. Blaabjerg, "Review on advanced control technologies for bidirectional DC/DC converters in DC microgrids," *IEEE J. Emerg. Sel. Topics Power Electron.*, vol. 9, no. 2, pp. 1205–1221, Apr. 2021.

[6] Y. Xie, R. Ghaemi, J. Sun, and J. S. Freudenberg, "Model predictive control for a full bridge DC/DC converter," *IEEE Trans. Control Syst. Technol.*, vol. 20, no. 1, pp. 164–172, Jan. 2012.

[7] S. J. Qin and T. A. Badgwell, "A survey of industrial model predictive control technology," *Control Eng. Pract.*, vol. 11, no. 7, pp. 733–764, Jul. 2003.

[8] T. Geyer and D. E. Quevedo, "Performance of multistep finite control set model predictive control for power electronics," *IEEE Trans. Power Electron.*, vol. 30, no. 3, pp. 1633–1644, Mar. 2015.

[9] J. Scoltock, T. Geyer, and U. K. Madawala, "Model predictive direct power control for grid-connected NPC converters," *IEEE Trans. Ind. Electron.*, vol. 62, no. 9, pp. 5319–5328, Sep. 2015.

[10] M. M. Ismail, W. Xu, J. Ge, Y. Tang, A. K. Junejo, and M. G. Hussien, "Adaptive linear predictive model of an improved predictive control of permanent magnet synchronous motor over different speed regions," *IEEE Trans. Power Electron.*, vol. 37, no. 12, pp. 15338–15355, Dec. 2022.

[11] R. Errouissi, A. Al-Durra, and S. M. Muyeen, "A robust continuous-time MPC of a DC–DC boost converter interfaced with a grid-connected photovoltaic system," *IEEE J. Photovolt.*, vol. 6, no. 6, pp. 1619–1629, Nov. 2016.

[12] S. Kwak, U. -C. Moon, and J.-C. Park, "Predictive-control-based direct power control with an adaptive parameter identification technique for improved AFE performance," *IEEE Trans. Power Electron.*, vol. 29, no. 11, pp. 6178–6187, Nov. 2014.

[13] T. Dorfling, H. du Toit Mouton, T. Geyer, and P. Karamanakos, "Long-horizon finite-control-set model predictive control with nonrecursive sphere decoding on an FPGA," *IEEE Trans. Power Electron.*, vol. 35, no. 7, pp. 7520–7531, Jul. 2020.

[14] R. O. Ramírez et al., "Finite-state model predictive control with integral action applied to a single-phase Z-source inverter," *IEEE J. Emerg. Sel. Topics Power Electron.*, vol. 7, no. 1, pp. 228–239, Mar. 2019.
[15] M. E. Albira and M. A. Zohdy, "Adaptive model predictive control for DC-DC power converters with parameters' uncertainties," *IEEE Access*, vol. 9, pp. 135121–135131, 2021.
[16] X. Liu, L. Qiu, Y. Fang, K. Wang, Y. Li, and J. Rodríguez, "A fuzzy approximation for FCS-MPC in power converters," *IEEE Trans. Power Electron.*, vol. 37, no. 8, pp. 9153–9163, Aug. 2022.
[17] B. Zhu, Z. Zheng, and X. Xia, "Constrained adaptive model-predictive control for a class of discrete-time linear systems with parametric uncertainties," *IEEE Trans. Autom. Control*, vol. 65, no. 5, pp. 2223–2229, May 2020.
[18] K. Yin, L. Gao, R. Chen, Z. Feng, and S. Liu, "Adaptive deadbeat predictive current control for PMSM with feed forward method," *IEEE Access*, vol. 9, pp. 101300–101310, 2021.
[19] X. An, G. Liu, Q. Chen, W. Zhao, and X. Song, "Adjustable model predictive control for IPMSM drives based on online stator inductance identification," *IEEE Trans. Ind. Electron.*, vol. 69, no. 4, pp. 3368–3381, Apr. 2022.
[20] W. Wu et al., "Data-driven iterative learning predictive control for power converters," *IEEE Trans. Power Electron.*, vol. 37, no. 12, pp. 14028–14033, Dec. 2022.
[21] O. Babayomi et al., "Adaptive predictive control with neuro-fuzzy parameter estimation for microgrid grid-forming converters," *Sustainability*, vol. 13, no. 13, 2021.
[22] L. Wang, Y. Wang, C. Liu, D. Yang, and Z. Chen, "A power distribution strategy for hybrid energy storage system using adaptive model predictive control," *IEEE Trans. Power Electron.*, vol. 35, no. 6, pp. 5897–5906, Jun. 2020.
[23] Y. Yang, S. -C. Tan, and S. Y. R. Hui, "Adaptive reference model predictive control with improved performance for voltage-source inverters," *IEEE Trans. Control Syst. Technol.*, vol. 26, no. 2, pp. 724–731, Mar. 2018.
[24] J. Zhidong et al., "An adaptive model predictive control for DC-DC boost converters," *Proc. CSEE*, vol. 38, no. 19, pp. 5838–5941, Oct. 2018.
[25] L. Po, L. Ruiyu, S. Tianying, Z. Jingrui, and F. Zheng, "Composite adaptive model predictive control for DC–DC boost converters," *IET Power Electron.*, vol. 11, no. 10, pp. 1706–1717, Aug. 2018.
[26] H. Makhamreh, M. Trabelsi, O. Kükrer, and H. Abu-Rub, "A Lyapunov-based model predictive control design with reduced sensors for a PUC7 rectifier," *IEEE Trans. Ind. Electron.*, vol. 68, no. 2, pp. 1139–1147, Feb. 2021.
[27] J. Yang, W. X. Zheng, S. Li, B. Wu, and M. Cheng, "Design of a prediction-accuracy-enhanced continuous-time MPC for disturbed systems via a disturbance observer," *IEEE Trans. Ind. Electron.*, vol. 62, no. 9, pp. 5807–5816, Sep. 2015.
[28] W.-H. Chen, D. J. Ballance, and P. J. Gawthrop, "Optimal control of nonlinear systems: A predictive control approach," *Automatica*, vol. 39, no. 4, pp. 633–641, 2003.
[29] F. Wang, L. He, J. Kang, R. Kennel, and J. Rodriguez, "Adaptive model predictive current control for PMLSM drive system," *IEEE Trans. Ind. Electron.*, to be published, doi: 10.1109/TIE.2022.3179550.
[30] J. Wang and L. Yu, "Adaptive resonant EIDO based optimized position precision control for magnetic levitation system," *IEEE Trans. Ind. Electron.*, 2022, to be published, doi: 10.1109/TIE.2022.3186348.

Hongyu Zhang (Student Member, IEEE) received the master's degree in electrical engineering in 2021 from Northwestern Polytechnical University, Xi'an, China, where he is currently working toward the Ph.D. degree in electrical engineering.

His current research interests include power system, optimal control, and power electronics.

Yuren Li received the master's degree in electrical engineering in 1989 from Northwestern Polytechnical University (NPU), Xi'an, China, where he received the Ph.D. degree in detection technology and automation device, in 2006.

He is currently a Full Professor with the School of Automation with NPU. His main research interests include aircraft brake control, power system, and automation technology.

Renyou Xie (Student Member, IEEE) received the master's degree in electrical engineering in 2021 from Northwestern Polytechnical University, Xi'an, China, where he received the Ph.D. degree in electrical engineering.

His current research interests include fuel cells, machine learning, and distributed optimization.

Jian Song (Student Member, IEEE) received the bachelor's and master's degrees in electrical engineering in 2021 from Northwestern Polytechnical University, Xi'an, China, where he is currently working toward the master's degree in electrical engineering.

His current research interests include energy management strategies and renewable energy technologies.

Bo Liang received the Ph.D. degree in detection technology and automation device from Northwestern Polytechnical University (NPU), Xi'an, China, in 2014.

He is currently an Associate Research Fellow with the School of Automation, NPU. His main research interests include measurement and control technology, electric power system, and power electronics.

Yigeng Huangfu (Senior Member, IEEE) received the M.S. and Ph.D. degrees in electrical engineering from Northwestern Polytechnical University (NPU), Xi'an, China, in 2007 and 2009, and the Ph.D. degree from the University of Technology of Belfort-Montbéliard, Belfort, France, in 2010.

He has been a Full Professor with NPU. He is also the Chair of IEEE IES Technical Committee on Transportation Electrification. His main research interests include power electrical conversion, transportation electrification, intelligence control of new energy conversion and renewable energy generation technology.

Dr. Huangfu is an Associate Editor for IEEE INDUSTRIAL ELECTRONICS APPLICATION and *IET Power Electronics*.